Adaptive Finite Element Method for Simulating Crack Propagation Using the Phase Field Model in Three-Dimensional Domains

Sayahdin Alfat[1], Asrun Safiuddin[2], Naim Naim[1], Mardiana Na-pirah[1]
Abdin Abdin[2] and Kasman Kasman[2]

[1] Physics Education Department, Halu Oleo University, Kendari, Southeast Sulawesi, Indonesia
[2] Vocational Engineering Education Department, Halu Oleo University, Kendari, Southeast Sulawesi, Indonesia
sayahdin.alfat@yahoo.com

Abstract. Research on crack propagation using the *phase field model* has gained significant attention in recent years. However, several aspects remain unexplored, such as crack propagation in three-dimensional domains. This study aims to model crack growth in three-dimensional domains using the phase field model. In this work, the three-dimensional domain is considered as a homogeneous and isotropic material. To solve the crack propagation equations, we employ the anisotropic adaptive finite element method, which is effectively implemented using the FreeFEM software. The results of this study demonstrate that an initially inclined crack rotates and becomes horizontal as it propagates, indicating a Mixed Mode Crack. This study provides qualitative results consistent with other research that does not utilize the anisotropic adaptive finite element method.

Keywords: Phase Field Model, Crack Propagation, Adaptive Finite Element Method, 3D, Mixed Mode, FreeFEM.

1 Introduction

One of the most popular continuous approaches today is the Phase Field Model (PFM). Since it does not require specific algorithms to determine crack paths and directions, this model simplifies the modeling of crack propagation. Initially, this model was proposed and introduced by Bourdin et al. [1]. Subsequently, it was extended and applied to study various multi-physics crack phenomena, such as cracks induced by heat [2-5], fluid pressure [6-9], hydrogen diffusion [3,10], and others. Additionally, this model has been employed to investigate crack behavior in various types of materials, including viscoelasticity [3,11-13], plasticity [14,15], heterogeneous and anisotropic materials [16,17], and thin plates [18].

Despite its robustness, this model has limitations when applied using grid-based numerical methods. The grid mesh size must be at least four times smaller than ϵ [19]. This requirement significantly increases the number of mesh elements, which, in turn,

S. Alfat et al. (eds.), *Proceedings of the 3rd International Conference on Mathematics and Science Education (ICMSE 2024)*, Advances in Social Science, Education and Humanities Research 922,
https://doi.org/10.2991/978-2-38476-402-0_10

lengthens computation time. This limitation is one of the main reasons why this model is rarely applied to certain cases involving three-dimensional domains. Therefore, one alternative method is the adaptive mesh refinement technique.

The adaptive mesh refinement method is a highly powerful and effective approach for reducing computation time [3,13]. This method can be applied to studies of cracks in both 2D domains [3-5,13] and 3D domains [13]. Specifically, within the context of the finite element method, this approach is referred to as the adaptive finite element method. In general, although this method is categorized into isotropic adaptive mesh and anisotropic adaptive mesh, the use of anisotropic adaptive mesh is less widespread compared to isotropic adaptive mesh. However, when the two are compared, the computation time for anisotropic adaptive mesh is significantly shorter [13,20]. Therefore, applying this method to 3D crack cases is highly practical. As additional information, to date, no studies have employed this method for crack simulations in 3D domains, except for research on cracks caused by fluid pressure conducted by Alfat [9].

Considering the various facts outlined in the previous two paragraphs, this study aims to model crack propagation using the Phase Field Model (PFM) approach. In this research, our primary focus is to apply the anisotropic adaptive finite element method to solve the general equations of crack propagation in cases involving three-dimensional domains.

The article is structured into five sections. Section two explains the linear elasticity equations and the modified linear elasticity equations based on damage variables. This section will also derive the equations governing the damage variables through the Microforce Balance approach. Section three discusses the computational methods, such as dimensionless transformations, weak forms, and time discretization, as well as computational setup and domains. An explanation of simulation results and a brief discussion are provided in section four. The final section covers conclusions and future perspectives of this research.

2 Governing Equation

2.1 Linear elastic equation

We consider a closed domain $\Omega \in R^d$ $(d = 2,3)$ containing a sharp crack Σ. Additionally, this domain is bounded by two types of boundaries, $\Gamma \coloneqq \partial\Omega = \Gamma_D^u \cup \Gamma_N^u$, namely the Dirichlet boundary Γ_D^u and the Neumann boundary Γ_N^u. A complete illustration of this is shown in Fig. 1 (left). Referring to the linear elasticity equations under quasi-static and isothermal conditions, the force balance equation for the domain Ω with a crack Σ can be written as follows:

$$\begin{cases} -\mathrm{div}(\sigma[\mathrm{u}]) = f(x) & x \in \Omega/\Sigma, \\ \sigma[u]n = q(x) & \text{on } \Gamma_{\mathrm{N}}^{\mathrm{u}}, \\ \sigma[u]n = 0 & \text{on } \Sigma^{\pm}, \\ \mathrm{u} = u_D(x,t) & \text{on } \Gamma_{\mathrm{D}}^{\mathrm{u}}. \end{cases} \tag{1}$$

Here, $x = (x_1, \cdots, x_d)^T$, $u = (u_1, \cdots, u_d)^T$, $f(x)$, n and t represent the position vector [m], displacement vector [m], body force [Pa m^{-1}], normal vector, and time [s], respectively. Additionally, $\sigma[u]$ and $e[u]$ denote the stress tensor [Pa] and strain tensor, respectively, which are defined as follows:

$$\sigma[u] \coloneqq Ce[u] = \lambda \mathrm{div} u I + 2\mu e[u]$$

$$e[u] \coloneqq \frac{1}{2}(\nabla u^T + (\nabla u^T)^T)$$

Parameter C is the elasticity tensor depending on the Lame constants $\lambda = \frac{E\nu}{(1+\nu)(1-2\nu)}$ and $\mu = \frac{E}{2(1-\nu)}$. Additionally, $\Sigma^{\pm}$ represents the two sides of the crack mouth Σ.

Essentially, Equation (1) can be obtained by differentiating the elastic energy function.

$$\mathcal{E}_{e\ell}(u) \coloneqq \frac{1}{2}\int_{\Omega} \sigma[u] : e[u] dx, \tag{2}$$

where $dx = dx_1 dx_2$ for 2D or $dx = dx_1 dx_2 dx_3$ for 3D. We will not show the derivation here, but readers can refer to the study conducted by one of our authors [3] for further details.

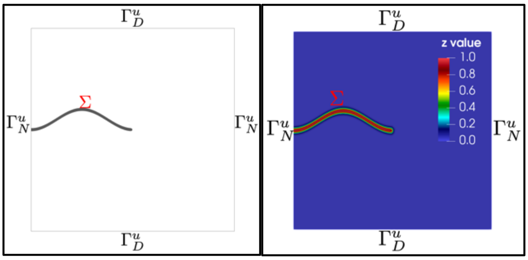

Fig. 1. Illustration of Ω with a sharp crack (left), and Ω with an approximated crack depending on z (right).

Directly, Equation (1) can be used to model and simulate crack propagation. However, this requires a complex algorithm, and naturally, this can be somewhat complicated. Therefore, Equation (1) needs to be modified.

Consider a damage variable (or PFM for crack propagation) $z \in (0,1)$ which represents a sharp crack Σ, where $z = 0$ denotes the non-cracked region and $z = 1$ denotes the cracked region. Clearly, the reader can see the illustration in Fig. 1 (right). Thus, Equation (1) can be modified as follows:

$$\begin{cases} -\mathrm{div}((1-z)^2\sigma[u]) = f(x) & x \in \Omega, \\ (1-z)^2\sigma[u]n = q(x) & \text{on } \Gamma_N^u, \\ u = u_D(x,t) & \text{on } \Gamma_D^u, \end{cases} \tag{3}$$

whereas, the elastic energy functional in Equation (2) can be modified as:

$$\mathcal{E}_{e\ell}^{*}(u) \coloneqq \frac{1}{2}\int_{\Omega}(1-z)^2\sigma[u]:e[u]dx. \tag{4}$$

Here, if the stress tensor is modified as $(1-z)^2\sigma[u] = (1-z)^2 Ce[u]$, it indicates that the elastic tensor C depends on the variable z.

If the variable z depends on time t, Equation (3) alone is not sufficient. Therefore, an evolution equation for crack propagation is required. We will detail this in the following section.

2.2 PFM for fracture

To determine the evolution equation for z, we consider the total energy:

$$E_{tot}(u,z) \coloneqq \mathcal{E}_{e\ell}^{*}(u) + E_s(z), \tag{5}$$

where it represents the total energy regulation proposed initially by Ambrosio-Tortorelli [21]. $\mathcal{E}_{e\ell}^{*}(u)$ is the modified elastic energy defined in Equation (4), and $E_s(z)$ is the surface energy defined as follows:

$$E_s(z) \coloneqq \frac{1}{2}\int_{\Omega}\gamma_*(x)\left(\epsilon|\nabla z|^2 + \frac{1}{\epsilon}z^2\right)dx, \tag{6}$$

where the variables $\gamma_*(x)$ and ϵ represent the critical energy release rate [Pa·m] and the length scale in the phase field model [m], respectively.

Applying the Gradient Flow method [3] or the Microforce Balance approach [5, 22], the evolution equation for crack propagation can be derived as follows:

$$\begin{cases} \alpha\dfrac{\partial z}{\partial t} = \left(\epsilon \operatorname{div}(\gamma_*(x)\nabla z) - \dfrac{\gamma_*(x)}{\epsilon}z + \sigma[u]:e[u](1-z)\right)_+ & x \in \Omega, \\ \dfrac{\partial z}{\partial n} = 0 & \text{on } \Gamma. \end{cases} \tag{7}$$

Here, α is the time regularization parameter for PFM [Pa·s]. The symbol $(\ )_+$ indicates that Equation (7) is irreversible. We will not explain how to derive Equation (7) using the Gradient Flow method. Readers can refer to [3] for more details. However, we will explain the derivation of this equation through the Microforce Balance approach.

Consider a Helmholtz free energy function under isothermal conditions, which is the sum of the elastic energy density function and the surface energy.

$$\Psi \coloneqq \frac{1}{2}(1-z)^2\sigma[u]:\mathrm{e}[u] + \frac{1}{2}\gamma_*(x)\left(\epsilon|\nabla z|^2 + \frac{1}{\epsilon}z^2\right), \tag{8}$$

and the (pseudo) dissipation energy function is defined as:

$$\Phi \coloneqq \frac{1}{2}\mathcal{D} = \frac{1}{2}\alpha|\dot{z}|^2. \tag{9}$$

See the explanation on how to derive the dissipation energy function $\mathcal{D}$ in [3,4]. Thus, we obtain two microscopic internal force functions as follows:

$$B^* := \frac{\partial \Psi}{\partial z} + \frac{\partial \Phi}{\partial \dot{z}} = \frac{\gamma_*(x)}{\epsilon} z - (1-z)\sigma[u]: e[u] + \alpha \dot{z}, \tag{10}$$

$$H^* := \frac{\partial \Psi}{\partial \nabla z} + \frac{\partial \Phi}{\partial \nabla \dot{z}} = \gamma_*(x)\epsilon \nabla z. \tag{11}$$

Since we are considering the Microforce Balance approach, neglecting micro-inertia effects [22], the first line of Equation (7) is obtained:

$$B^* - \mathrm{div} H^* = 0$$

$$\alpha \dot{z} = \epsilon \mathrm{div}(\gamma_*(x)\nabla z) - \frac{\gamma_*(x)}{\epsilon} z + (1-z)\sigma[u]: e[u].$$

Finally, we derive the first line of Equation (7).

The equations (3) and (7) refer to the Phase Field Model (PFM) equations for crack propagation. These equations were introduced by Takaishi and Kimura [3]. We will use these equations to simulate crack propagation in a 3D domain.

3 Computational Method

3.1 Non-dimensional trasformation

To simplify the computation of Equations (3) and (7), we transform these equations into non-dimensional forms. Let us consider the following non-dimensional variables:

$$\tilde{x} = \frac{x}{c_x}, \quad \tilde{u} = \frac{u}{c_u}, \quad \tilde{E} = \frac{E}{c_e}, \quad \tilde{\epsilon} = \frac{\epsilon}{c_x}, \ \tilde{\gamma}_* = \frac{c_x}{c_u^2 c_e}\gamma_*, \tag{12}$$

where the variables denoted by $\sim$ are non-dimensional variables. Here, c_x, c_u, and c_e represent positive constants. Substituting Equation (12) into Equations (3) through (7), we obtain the non-dimensional forms of Equations (3) and (7) as follows:

$$\begin{cases} -\widetilde{\mathrm{div}}((1-z)^2\sigma[\tilde{u}]) = \tilde{f}(\tilde{x}) & \tilde{x} \in \tilde{\Omega}, \\ \tilde{\alpha}\frac{\partial z}{\partial t} = \left(\tilde{\epsilon}\widetilde{\mathrm{div}}\big(\tilde{\gamma}_*(\tilde{x})\tilde{\nabla} z\big) - \frac{\tilde{\gamma}_*(\tilde{x})}{\tilde{\epsilon}} z + \sigma[\tilde{u}]: e[\tilde{u}](1-z)\right)_+ & \tilde{x} \in \tilde{\Omega}, \\ (1-z)^2\sigma[\tilde{u}]n = q(\tilde{x}) & \text{on } \Gamma_N^u, \\ \tilde{u} = u_D(\tilde{x}, t) & \text{on } \Gamma_D^u, \\ \frac{\partial z}{\partial n} = 0 & \text{on } \Gamma. \end{cases} \tag{13}$$

The initial condition for z is defined as $z|_{t=0} = z^0(\tilde{x})$. We will not elaborate in detail on the derivation of Equation (13). However, readers can find a clear explanation in [9]. For convenience, the symbol $\sim$ and the variable $\tilde{f}(\tilde{x})$ in Equation (13) will be omitted when constructing the weak form and performing time discretization.

3.2 Time discretization and weak form

This section will explain the time discretization and the weak form for Equation (13). The study employs a semi-implicit time scheme to compute Equation (13) as follows:

$$\begin{cases} -\mathrm{div}\big((1-z^{k-1})\sigma[u^k]\big) = 0 & x \in \Omega, \\ \alpha\frac{\tilde{z}^k - z^{k-1}}{\Delta t} = \epsilon \mathrm{div}(\gamma_* \nabla \tilde{z}^k) - \frac{\gamma_*}{\epsilon}\tilde{z}^k + (1-\tilde{z}^k)\sigma[u^{k-1}]: e[u^{k-1}] & x \in \Omega, \\ z^k = \max(\tilde{z}^k, z^{k-1}) & x \in \Omega, \\ (1-z^{k-1})\sigma[u^k]n = 0 & \text{on } \Gamma_N^u, \\ u^k = u_D^k & \text{on } \Gamma_D^u, \\ \frac{\partial \tilde{z}^k}{\partial n} = 0 & \text{on } \Gamma. \end{cases} \tag{14}$$

Let u^k and z^k represent an approximation solution for the variables u and z at time $t = k\Delta t$ $(k = 1,2,\cdots,\mathrm{t_{max}})$. Here, Δt is a constant time increment. Additionally, $\max(\tilde{z}^k, z^{k-1})$ denotes the symbol $(\quad)_+$ in the second line of Equation (13). Finally, we have set up the time discretization form for Equation (13). Next, we will present the weak form of Equation (14).

Consider two functions (w, v) that serve as sequential test functions for u and z, respectively, as follows:

$$\mathrm{V^u} := (w \in H^1(\Omega) | w = 0 \text{ on } \Gamma_D),$$

$$V^z := (v \in H^1(\Omega) | v = 0 \text{ on } \Gamma),$$

where $H^1(\Omega)$ denotes the Sobolev space. When these test functions are multiplied by the equations in the first and second lines of Equation (14), and each term is integrated, we obtain the weak form of Equation (14) as follows:

$$a_u(u^k, w) = l_u^k(w) \quad (\forall \mathrm{w} \in \mathrm{V^u}), \tag{15}$$

$$a_z(z^k, v) = l_z^k(v) \ (\forall v \in V^z), \tag{16}$$

where

$$a_u(u^k, w) := \int_\Omega (1 - z^{k-1})^2\, \sigma[u^k]: e[w] dx,$$

$$l_u^k(w) \ := \ 0,$$

$$a_z(z^k, v) := \int_\Omega \left(\frac{\alpha}{\Delta t} + \frac{\gamma_*}{\epsilon} + W(u^{k-1})\right) \tilde{z}^k v \, dx + \epsilon \int_\Omega \gamma_* \, \nabla z \cdot \nabla v d,$$

$$l_z^k(v) := \int_\Omega \left(\frac{\alpha}{\Delta t} z^{k-1} + W(u^{k-1})\right) v \, dx,$$

We will use Equations (15)-(16) to compute the numerical solution of Equation (13).

3.3 Domain setting

In this section, we present the computational setup and domain, including the physical parameters used in this study. One challenge in modeling crack propagation using the phase field model is that the size of each triangular mesh, $h(\mathcal{T}_{\hbar})$, within the domain must be four times smaller than ϵ [13,19]. Consequently, the number of meshes increases significantly, which eventually results in longer computation times. To address this, the numerical method used in this study is the anisotropic adaptive finite element method. This approach allows us to adjust the size and number of triangular meshes depending on the function z (see Fig. 2). As a result, the computation time will be considerably faster [13,20].

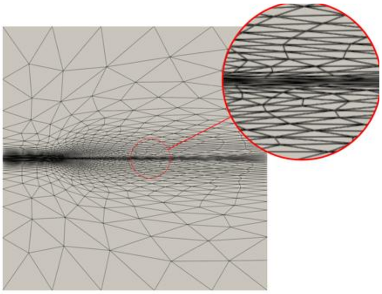

Fig. 2. Illustration of the anisotropic adaptive finite element method on a 2D domain with a straight crack. The mesh size is very small and numerous in the crack area [13].

Overall, the code was written using FreeFEM software [23] and run on a computer with specifications of an Intel(R) Core i9-12900 kHz, a 24-core processor, and 94.0 GB of RAM. For simplicity, we present a pseudocode for calculating Equations (15)-(16) in the table below. Visualization of calculation results using the ParaView software.

Algorithm 1: Adaptive Mesh-Based Crack Propagation Model

Input: physical parameters

Input: time parameters t_{max} **and** Δt

Set: initial mesh $\mathcal{T}_{\hbar}^{0}$ and initial crack $z^{0}(x)$

For $k = 1, \cdots, T/\Delta t$ **do**

  Set $\mathcal{T}_{\hbar}^{k} = \mathcal{T}_{\hbar}^{k-1}$

```
    Calculate solution u^k and z^k using equations
    (15)-(16)

    For i = 1,⋯,10 do

        Design new mesh T_h^i based on  z^k

    End for

    Set T_h^k = T_h^i

End for
```

Table 1. Physical an time parameters.

Phy. Par.	Value	Phy. Par.	Value
E	50	α	0.001
ν	0.29	h_{min}	0.0005
γ_*	0.5	Δt	0.0005
ϵ	0.05	t	0.5

Since we are using non-dimensional variables, the physical parameters are also set as non-dimensional. The parameters used in this study are shown in Table 1.

As mentioned in the Introduction, this study focuses on simulating crack propagation in a 3D domain. Therefore, we define the domain as $\Omega := \Omega' \times (0,0.5) \in R^3$ with $\Omega' := (0,2)^2 \in R^2$, which contains initial cracks. There are two cases: the first case is a domain with one initial crack, and the second case has two initial cracks. Both cases have an initial crack length of 0.5 with an inclination of $\theta = 45^o$. In each case, the top and bottom surfaces are subjected to traction. For clarity, this is illustrated in Fig. 3.

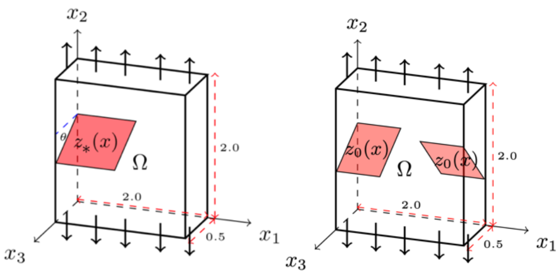

Fig. 3. Illustration of the three-dimensional domain. The red area represents the initial crack with an inclination of $\theta = 45^o$.

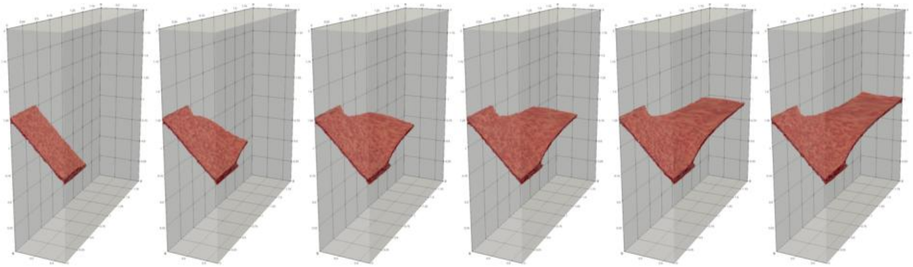

Fig. 4. The crack propagation profile in the three-dimensional domain during the time interval t = 0, 0.25, 0.335, 0.35, 0.375, 0.4 (from left to right).

4 Result and Discussion

The simulation results of crack propagation in a 3D domain with one initial crack are shown in Fig. 4. This figure is a snapshot of each crack propagation process at times t = 0, 0.25, 0.335, 0.35, 0.375, 0.4. From this figure, it can be seen that the initially inclined crack gradually rotates as it propagates until it reaches t = 0.335. Meanwhile, between the time intervals 0.335 < t < 0.4, the crack grows planar (or perpendicular to the tensile force). For further details, readers can view the video we uploaded at https://zenodo.org/records/10695316/files/Single.avi?download=1. Additionally, the domain is fully divided (completely damaged) at t ≈ 0.38 . This is shown in Fig. 5, where the blue line graph appears flat at t ≈ 0.38. The illustration of the fully damaged domain is shown in Fig. 6 (left).

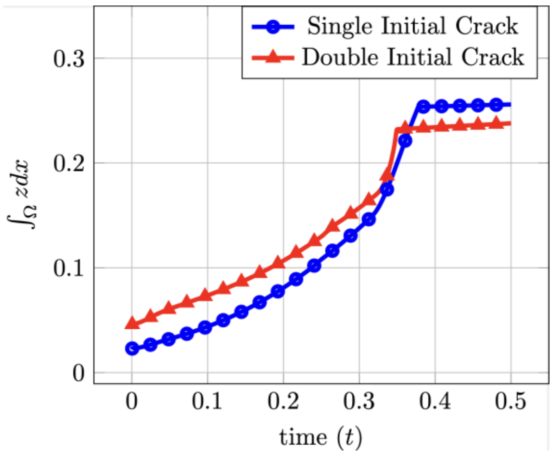

Fig. 5. Evolution profile of the crack area $\int_\Omega z dx$ at each time step for domains with 1 initial crack and 2 initial cracks.

For the second case, simulation results in the form of snapshots for each time increment are not shown. However, they are provided in a video available at https://zenodo.org/records/10695316/files/Double.avi?download=1. Overall, the crack behavior is almost identical to the first case. Cracks at both ends of the initial crack rotate and eventually merge into a single crack at t ≈ 0.35 (see Fig. 6 (right)). This is clearly illustrated in Fig. 5.

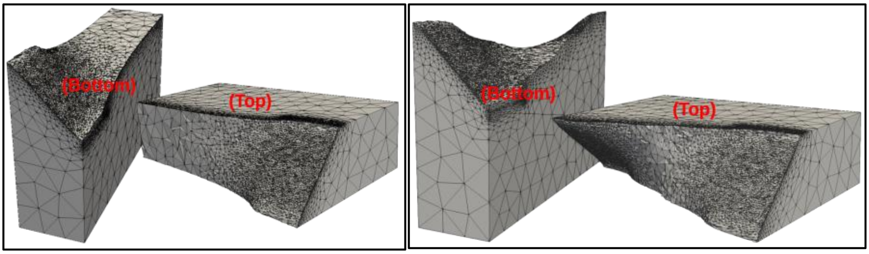

Fig. 6. Mesh profile for each segment of the domain. The left and right sections represent domains with 1 initial crack and two initial cracks, respectively. This profile was obtained using ParaView software.

The phenomenon of crack rotation can be explained as follows. Under conditions where the domain is subjected to pure tensile stress, the resulting crack profile will be perpendicular to the direction of the tensile force. If the domain contains an initially inclined crack, the crack will rotate until it aligns with the direction of the tensile force. This condition is classified as a mixed-mode crack (Mode I/III). This phenomenon was observed in both of our cases, where the crack rotated and ceased propagating once it became perpendicular to the direction of the tensile force.

Qualitatively, our results for the first case show similarities with both experimental studies [24-27] and computational studies [3]. For the second case, although neither computational nor experimental studies have investigated it yet, we believe and suspect that the results will be consistent with both experimental and computational findings, given the results of the first case as a reference.

5 Conclusion and Future Perspectives

The study on crack propagation in three-dimensional domains using the Phase Field Model (PFM) and anisotropic adaptive finite element method has been successfully conducted. The use of PFM for crack propagation simulation clearly facilitates our understanding of this phenomenon. This model allows us to simulate crack propagation without the need for complex or specialized algorithms, even within three-dimensional domains. Moreover, the application of the anisotropic adaptive finite element method results in smooth crack paths and relatively shorter computation times.

One thing that we can conclude from this study is that when a domain with an inclined initial crack is subjected to a tensile force, the crack profile rotates and becomes horizontal as the crack propagates, indicating a Mixed Mode Crack. Qualitatively, the results of this study are consistent with previous research [3,24-27].

We consider this research a preliminary study. Therefore, we plan to extend this research to observe crack propagation in various cases, such as cracks due to compressive, tensile, or shear forces. Of course, we will use a 3D domain to produce more realistic results. Additionally, we also plan to test our second case using an experimental approach.

Acknowledgments. This research was not funded by any grant.

Disclosure of Interests. The authors have no competing interests to declare that are relevant to the content of this article.

References

1. B. Bourdin, "Numerical implementation of the variational formulation for quasi-static brittle fracture," Interfaces and Free Boundaries, pp. 411–430, 2007, doi: https://doi.org/10.4171/ifb/171
2. B. Bourdin, J.-J. Marigo, C. Maurini, and P. Sicsic, "Morphogenesis and Propagation of Complex Cracks Induced by Thermal Shocks," Physical Review Letters, vol. 112, no. 1, Jan. 2014, doi: https://doi.org/10.1103/physrevlett.112.014301.
3. M. Kimura, Takeshi Takaishi, Sayahdin Alfat, T. Nakano, and Y. Tanaka, "Irreversible phase field models for crack growth in industrial applications: thermal stress, viscoelasticity, hydrogen embrittlement," SN Applied Sciences, vol. 3, no. 9, Aug. 2021, doi: https://doi.org/10.1007/s42452-021-04593-6.
4. Sayahdin Alfat, M. Kimura, and Alifian Maulana, "Phase Field Models for Thermal Fracturing and Their Variational Structures," Materials, vol. 15, no. 7, pp. 2571–2571, Mar. 2022, doi: https://doi.org/10.3390/ma15072571.
5. Sayahdin Alfat, "New frameworks of PFM for thermal fracturing in the linear thermoelasticity solids based on a microforce balance approach," Physica D Nonlinear Phenomena, pp. 134498–134498, Jan. 2025, doi: https://doi.org/10.1016/j.physd.2024.134498.
6. A. Mikelić, M. F. Wheeler, and T. Wick, "Phase-field modeling of a fluid-driven fracture in a poroelastic medium," Computational Geosciences, vol. 19, no. 6, pp. 1171–1195, Nov. 2015, doi: https://doi.org/10.1007/s10596-015-9532-5.
7. Z. S. Wilson and C. M. Landis, "Phase-field modeling of hydraulic fracture," vol. 96, pp. 264–290, Nov. 2016, doi: https://doi.org/10.1016/j.jmps.2016.07.019.
8. Chukwudi Paul Chukwudozie, Blaise Bourdin, and K. Yoshioka, "A variational phase-field model for hydraulic fracturing in porous media," Computer Methods in Applied Mechanics and Engineering, vol. 347, pp. 957–982, Apr. 2019, doi: https://doi.org/10.1016/j.cma.2018.12.037.
9. Alfat, S. (2023). Phase Field Model for Crack Propagation and its Extension to Thermoelasticity and Poroelasticity: Thermal Fracturing, Hydraulic Fracturing, and Desiccation Cracking (Doctoral dissertation, Ph. D. thesis, Kanazawa University).
10. T. K. Mandal, V. P. Nguyen, and J.-Y. Wu, "Comparative study of phase-field damage models for hydrogen assisted cracking," Theoretical and Applied Fracture Mechanics, vol. 111, pp. 102840–102840, Dec. 2020, doi: https://doi.org/10.1016/j.tafmec.2020.102840.

11. Z. Liu, J. Roggel, and D. Juhre, "Phase-Field Modelling of Fracture in Viscoelastic Solids," Procedia Structural Integrity, vol. 13, pp. 781–786, 2018, doi: https://doi.org/10.1016/j.prostr.2018.12.129.
12. B. Yin, J. Storm, and M. Kaliske, "Viscoelastic phase-field fracture using the framework of representative crack elements," International Journal of Fracture, vol. 237, no. 1–2, pp. 139–163, Mar. 2021, doi: https://doi.org/10.1007/s10704-021-00522-1.
13. Sayahdin Alfat, "On energy-consistency principle of PFM for thermal fracturing in thermoviscoelasticity solids and its application for modeling thermal response due to crack growth based on adaptive mesh technique," Computers & Mathematics with Applications, vol. 175, pp. 107–118, Sep. 2024, doi: https://doi.org/10.1016/j.camwa.2024.09.016.
14. F. P. Duda, A. Ciarbonetti, P. J. Sánchez, and A. E. Huespe, "A phase-field/gradient damage model for brittle fracture in elastic–plastic solids," International Journal of Plasticity, vol. 65, pp. 269–296, Feb. 2015, doi: https://doi.org/10.1016/j.ijplas.2014.09.005.
15. C. Schreiber, C. Kuhn, Ralf Müller, and T. I. Zohdi, "A phase field modeling approach of cyclic fatigue crack growth," International Journal of Fracture, vol. 225, no. 1, pp. 89–100, Jul. 2020, doi: https://doi.org/10.1007/s10704-020-00468-w.
16. T. T. Nguyen, J. Réthoré, and M.-C. Baietto, "Phase field modelling of anisotropic crack propagation," European Journal of Mechanics - A/Solids, vol. 65, pp. 279–288, Sep. 2017, doi: https://doi.org/10.1016/j.euromechsol.2017.05.002.
17. L. Schöller, D. Schneider, C. Herrmann, A. Prahs, and B. Nestler, "Phase-field modeling of crack propagation in heterogeneous materials with multiple crack order parameters," Computer Methods in Applied Mechanics and Engineering, vol. 395, p. 114965, May 2022, doi: https://doi.org/10.1016/j.cma.2022.114965.
18. F. Amiri, D. Millán, Y. R. Shen, Timon Rabczuk, and P. Moreno, "Phase-field modeling of fracture in linear thin shells," Theoretical and Applied Fracture Mechanics, vol. 69, pp. 102–109, Feb. 2014, doi: https://doi.org/10.1016/j.tafmec.2013.12.002.
19. C. Miehe, M. Hofacker, and F. Welschinger, "A phase field model for rate-independent crack propagation: Robust algorithmic implementation based on operator splits," Computer Methods in Applied Mechanics and Engineering, vol. 199, no. 45, pp. 2765–2778, Nov. 2010, doi: https://doi.org/10.1016/j.cma.2010.04.011.
20. N. Ferro, S. Micheletti, and S. Perotto, "Anisotropic mesh adaptation for crack propagation induced by a thermal shock in 2D," Computer Methods in Applied Mechanics and Engineering, vol. 331, pp. 138–158, Dec. 2017, doi: https://doi.org/10.1016/j.cma.2017.11.024.
21. L. Ambrosio and V. M. Tortorelli, "ON THE APPROXIMATION OF FREE DISCONTINUITY PROBLEMS," no. 1, pp. 105–123, Jan. 1992.
22. C. Kuhn, "Numerical and Analytical Investigation of a Phase Field Model for Fracture," Mar. 2013.
23. F. Hecht, "New development in freefem++," Journal of Numerical Mathematics, vol. 20, no. 3–4, Jan. 2012, doi: https://doi.org/10.1515/jnum-2012-0013.
24. M. F. Yaren, O. Demir, A. O. Ayhan, and S. İriç, "Three-dimensional mode-I/III fatigue crack propagation: Computational modeling and experiments," International Journal of Fatigue, vol. 121, pp. 124–134, Apr. 2019, doi: https://doi.org/10.1016/j.ijfatigue.2018.12.005.
25. B. Lin, M. E. Mear, and Krishnaswa Ravi-Chandar, "Criterion for initiation of cracks under mixed-mode I + III loading," International journal of fracture, vol. 165, no. 2, pp. 175–188, Jun. 2010, doi: https://doi.org/10.1007/s10704-010-9476-7.
26. V. Lazarus and J.-B. Leblond, "Propagation de fissures en mode mixte (I + III) ou (I + II + III)," Comptes Rendus de l'Académie des Sciences - Series IIB - Mechanics-Physics-Chemistry-Astronomy, vol. 326, no. 3, pp. 171–177, Mar. 1998, doi: https://doi.org/10.1016/s1251-8069(99)89004-6.

27. V. Lazarus, J.-B. Leblond, and Salah-Eddine Mouchrif, "Crack front rotation and segmentation in mixed mode I+III or I+II+III. Part II: Comparison with experiments," Journal of the Mechanics and Physics of Solids, vol. 49, no. 7, pp. 1421–1443, Jul. 2001, doi: https://doi.org/10.1016/s0022-5096(01)00008-4.